

Table 1 (Continued)

Monosaccharidic composition ^a				Theoretical mass ^b	Positive ion mode		Negative ion mode		Deduced structure ^d
dHex	Hex	HX	NA		Observed m/z^c	Retention time (min)	Observed m/z^c	Retention time (min)	
2	6	4	0	2096.78	1049.42(2)	15.97			
2	6	4	0	2096.78	1049.42(2)	16.61			Hybrid, BisectGN
2	6	4	0	2096.78	1049.43(2)	25.73			
1	7	4	0	2112.77			1055.38(2)	34.62	
1	4	5	1	2120.79	1061.45(2)	20.43			Complex
1	4	5	1	2120.79	1061.45(2)	24.74	1059.39(2)	24.70	
1	4	5	1	2120.79	1061.45(2)	26.47	1059.39(2)	26.42	CoreF
2	5	5	0	2137.80	1069.94(2)	9.17			Lby
2	5	5	0	2137.80	1069.94(2)	21.30			
2	5	5	0	2137.80	1069.95(2)	23.09	1067.9(2)	23.04	
1	5	3	2	2167.78	1084.94(2)	30.41	1082.89(2)	30.37	Hybrid, CoreF
2	4	6	0	2178.83	1090.45(2)	26.08			
0	6	3	2	2183.77	1092.95(2)	28.63	1090.88(2)	28.60	Hybrid, diSia
0	5	4	2	2224.80	1113.45(2)	26.10			
2	5	4	1	2225.82	1113.95(2)	27.56			
2	5	4	1	2225.82	1113.98(2)	34.80			
1	6	4	1	2241.81	1121.95(2)	26.60	1119.90(2)	26.63	
1	6	4	1	2241.81			1119.90(2)	30.58	
1	6	4	1	2241.81			1119.91(2)	38.14	
3	6	4	0	2242.83	1122.46(2)	14.23			
2	7	4	0	2258.83	1130.46(2)	10.47			
3	5	5	0	2283.86	1142.96(2)	16.87			
1	4	6	1	2323.87	1162.98(2)	26.60			
1	6	3	2	2329.83			1163.91(2)	31.72	
1	6	3	2	2329.83			1163.91(2)	32.54	Hybrid, diSia
1	5	4	2	2370.86	1186.55(2)	29.89	1184.42(2)	30.00	Complex, CoreF
1	5	4	2	2370.86			1184.43(2)	36.00	
1	5	4	2	2370.86	1186.52(2)	36.31	1184.42(2)	36.40	Complex, CoreF
1	5	4	2	2370.86	1186.50(2)	42.47	1184.43(2)	42.43	Complex, CoreF
3	5	4	1	2370.86			1184.93(2)	30.99	
2	5	5	1	2428.90	1215.50(2)	21.17	1213.44(2)	21.25	
2	5	5	1	2428.90	1215.50(2)	23.84			
2	5	5	1	2428.90	1215.52(2)	26.32	1213.45(2)	26.28	
2	5	5	1	2428.90	1215.50(2)	27.50	1213.45(2)	27.53	
2	5	4	2	2516.91	1259.60(2)	32.23	1257.45(2)	32.19	Complex, Lax, CoreF, diSia
2	5	4	2	2516.91			1257.45(2)	36.72	
2	5	6	1	2631.98			876.32(3), 1314.99(2)	26.76	
3	5	4	2	2662.97			1330.49(2)	32.78	
1	5	6	2	2777.02			1387.50(2)	30.99	
0	6	5	3	2881.03			1439.50(2)	34.83	
0	6	5	3	2881.03			1439.49(2)	40.77	
2	6	5	2	2882.05			1440.05(2)	37.96	
2	6	6	2	3085.13			1541.55(2)	31.38	

^a dHex, deoxyhexose; Hex, hexose; HX, *N*-acetylhexamine; NeuAc, *N*-acetylneuramic acid.

^b Monoisotopic value.

^c Values in parentheses are charge state.

^d Structures are deduced by MSⁿ. Complex, complex-type-oligosaccharide; Hybrid, hybrid-type-oligosaccharide; M5-9, high-mannose-type oligosaccharide containing 5–9 mannose residues; BisectGN, bisecting GlcNAc; Lax, Lewis a/x structure; Lby, Lewis b/y structure; diSia, disialic acid.

^e Ammonium adducted form.

3.2.2.4. *NeuAc-Gal-GlcNAc*-. Fig. 7B shows the product ion spectrum of a disialylated oligosaccharide, NeuAc₂dHex₁Hex₅HexNAc₃HexNAc₁, at m/z 1187 (42.5 min). Although B ions were detected at m/z 454 (B_{2x}⁺), 657 (B_{3x}⁺) and 819 (B_{4x}⁺), none of the fragment ions at m/z 495 (NeuAc-GlcNAc⁺), 948 (NeuAc-Gal-(NeuAc-)GlcNAc⁺), or 1110 (NeuAc-Gal-(NeuAc-)GlcNAc-Man⁺) were detected in the spectrum. This result suggests that the two NeuAc residues occupy both non-reducing ends of the biantennary

form. Fucosylation of the inner trimannosyl core GlcNAc was determined by the detection of Y ions at m/z 370 (Y_{1α}⁺) and 1059 (Y_{4α/4β}⁺). These product ions lead to assignment of this oligosaccharide the structure in Fig. 6B.

3.2.2.5. (v) *NeuAc-NeuAc*-. Fig. 7C shows the product ion spectrum of a disialylated and difucosylated oligosaccharide, NeuAc₂dHex₂Hex₅HexNAc₃HexNAc₁, at m/z 1260 (32.2 min). The characteristic ions at m/z 583 (NeuAc-NeuAc⁺,

In these two studies, we have demonstrated a strategy for glycosylation analysis of Thy-1, including identification of a glycoprotein, determination of glycosylation sites, site-specific glycosylation analysis, and structural analysis of oligosaccharide details. This strategy can be applied to glycosylation analysis of other glycoproteins. Specifically, the glycoprotein sample is divided into two. One is subjected to proteinase digestion followed by peptide/glycopeptide mapping, which provides information on glycosylation sites and site-specific heterogeneity. The other is subjected to PNGase F digestion followed by mass spectrometric oligosaccharide profiling, by which a detailed structure of *N*-glycans released from a glycoprotein could be provided. Recently, proteomic approaches, which are based on two-dimensional electrophoresis followed by mass spectrometry, have been used in various fields. Although glycosylation analysis of abundant glycoproteins in gel has been successful, that of a low-abundance glycoprotein in gel remains a great challenge. The proposed method consisting of peptide/glycopeptide mapping followed by oligosaccharide profiling with sequential scans by IT-MS-FT-ICR-MS will likely be a powerful tool for glycosylation analysis of low-abundance glycoproteins and for proteomics/glycomics.

Acknowledgements

This work was supported in part by a Grant-in-Aid for Creative Scientific Research (16GS0313) from the Ministry of Education, Culture, Sports, and Technology, the Ministry of Health, Labor and Welfare, and Core Research for the Evolutional Science and Technology Program (CREST) of the Japan Science and Technology Agency (JST).

We appreciate Dr. A. Hachisuka of the National Institute of Health Science for her technical advice.

We thank Dr. M. Kubota and Mr. M. Yoshida of Thermo Electron K.K. (Japan) for their technical support.

References

- [1] A. Varki, *Glycobiology* 3 (1993) 97.
- [2] J.W. Dennis, M. Granovsky, C.E. Warren, *Biochim. Biophys. Acta* 1473 (1999) 21.
- [3] Y. Sato, M. Kimura, C. Yasuda, Y. Nakano, M. Tomita, A. Kobata, T. Endo, *Glycobiology* 9 (1999) 655.
- [4] G. Durand, N. Seta, *Clin. Chem.* 46 (2000) 795.
- [5] O. Krokhin, W. Ens, K.G. Standing, J. Wilkins, H. Perreault, *Rapid Commun. Mass Spectrom.* 18 (2004) 2020.
- [6] Y. Satomi, Y. Shimonishi, T. Takao, *FEBS Lett.* 576 (2004) 51.
- [7] Y. Wada, M. Tajiri, S. Yoshida, *Anal. Chem.* 76 (2004) 6560.
- [8] W. Chai, V. Piskarev, A.M. Lawson, *Anal. Chem.* 73 (2001) 651.
- [9] D. Sagi, J. Peter-Katalinic, H.S. Conradt, M. Nimtz, *J. Am. Soc. Mass Spectrom.* 13 (2002) 1138.
- [10] A. Zamfir, D.G. Seidler, H. Kresse, J. Peter-Katalinic, *Glycobiology* 13 (2003) 733.
- [11] D.J. Harvey, R.L. Martin, K.A. Jackson, C.W. Sutton, *Rapid Commun. Mass Spectrom.* 18 (2004) 2997.
- [12] C. Robbc, C. Capon, B. Coddeville, J.C. Michalski, *Rapid Commun. Mass Spectrom.* 18 (2004) 412.
- [13] N. Ojima, K. Masuda, K. Tanaka, O. Nishimura, *J. Mass Spectrom.* 40 (2005) 380.
- [14] C.W. Sutton, J.A. O'Neill, J.S. Cottrell, *Anal. Biochem.* 218 (1994) 34.
- [15] B. Küster, S.F. Wheeler, A.P. Hunter, R.A. Dwek, D.J. Harvey, *Anal. Biochem.* 250 (1997) 82.
- [16] B. Küster, T.N. Krogh, E. Mortz, D.J. Harvey, *Proteomics* 1 (2001) 350.
- [17] K. Hirayama, R. Yuji, N. Yamada, K. Kato, Y. Arata, I. Shimada, *Anal. Chem.* 70 (1998) 2718.
- [18] F. Wang, A. Nakouzi, R.H. Angelotti, A. Casadevall, *Anal. Biochem.* 314 (2003) 266.
- [19] K. Sandra, I. Stals, P. Sandra, M. Claeysens, J. Van Becumen, B. Devreese, *J. Chromatogr. A* 1058 (2004) 263.
- [20] Y. Satomi, Y. Shimonishi, T. Hase, T. Takao, *Rapid Commun. Mass Spectrom.* 18 (2004) 2983.
- [21] A. Harazono, N. Kawasaki, T. Kawanishi, T. Hayakawa, *Glycobiology* 15 (2005) 447.
- [22] M. Wührer, C.A. Kocleman, C.H. Hokke, A.M. Deelder, *Anal. Chem.* 77 (2005) 886.
- [23] B.L. Schulz, N.H. Packer, N.G. Karlsson, *Anal. Chem.* 74 (2002) 6088.
- [24] N.L. Wilson, B.L. Schulz, N.G. Karlsson, N.H. Packer, *J. Proteome Res.* 1 (2002) 521.
- [25] L.A. Gennaro, D.J. Harvey, P. Vouros, *Rapid Commun. Mass Spectrom.* 17 (2003) 1528.
- [26] N.G. Karlsson, B.L. Schulz, N.H. Packer, *J. Am. Soc. Mass Spectrom.* 15 (2004) 659.
- [27] N.G. Karlsson, N.L. Wilson, H.J. Wirth, P. Dawes, H. Joshi, N.H. Packer, *Rapid Commun. Mass Spectrom.* 18 (2004) 2282.
- [28] M. Wührer, C.A. Kocleman, A.M. Deelder, C.H. Hokke, *Anal. Chem.* 76 (2004) 833.
- [29] Y. Takegawa, K. Deguchi, S. Ito, S. Yoshioka, H. Nakagawa, S. Nishimura, *Anal. Chem.* 77 (2005) 2097.
- [30] S. Itoh, N. Kawasaki, M. Ohta, T. Hayakawa, *J. Chromatogr. A* 978 (2002) 141.
- [31] S. Itoh, N. Kawasaki, A. Harazono, N. Hashii, Y. Matsuishi, T. Kawanishi, T. Hayakawa, *J. Chromatogr. A* 1094 (2005) 105.
- [32] N. Kawasaki, M. Ohta, S. Hyuga, O. Hashimoto, T. Hayakawa, *Anal. Biochem.* 269 (1999) 297.
- [33] S. Itoh, N. Kawasaki, M. Ohta, M. Hyuga, S. Hyuga, T. Hayakawa, *J. Chromatogr. A* 968 (2002) 89.
- [34] N. Kawasaki, S. Itoh, M. Ohta, T. Hayakawa, *Anal. Biochem.* 316 (2003) 15.
- [35] C. Bordier, *J. Biol. Chem.* 256 (1981) 1604.
- [36] M.P. Lisanti, M. Sargiacomo, L. Graeve, A.R. Saltiel, E. Rodriguez-Boulan, *Proc. Natl. Acad. Sci. U.S.A.* 85 (1988) 9557.
- [37] B. Domon, C.E. Costello, *Glycoconjugate J.* 5 (1988) 397.
- [38] C. Sato, T. Matsuda, K. Kitajima, *J. Biol. Chem.* 277 (2002) 45299.

Site-specific glycosylation analysis of human apolipoprotein B100 using LC/ESI MS/MS

Akira Harazono¹, Nana Kawasaki, Toru Kawanishi,
and Takao Hayakawa

National Institute of Health Sciences, Division of Biological Chemistry
and Biologicals, 1-18-1 Kami-yoga, Setagaya-Ku, Tokyo 158-8501, Japan

Received on 28 June 2004; revised on 24 November 2004; accepted on
16 December, 2004

Human apolipoprotein B100 (apoB100) has 19 potential *N*-glycosylation sites, and 16 asparagine residues were reported to be occupied by high-mannose type, hybrid type, and monoantennary and biantennary complex type oligosaccharides. In the present study, a site-specific glycosylation analysis of apoB100 was carried out using reversed-phase high-performance liquid chromatography coupled with electrospray ionization tandem mass spectrometry (LC/ESI MS/MS). ApoB100 was reduced, carboxymethylated, and then digested by trypsin or chymotrypsin. The complex mixture of peptides and glycopeptides was subjected to LC/ESI MS/MS, where product ion spectra of the molecular ions were acquired data-dependently. The glycopeptide ions were extracted and confirmed by the presence of carbohydrate-specific fragment ions, such as *m/z* 204 (HexNAc) and 366 (HexHexNAc), in the product ion spectra. The peptide moiety of glycopeptide was determined by the presence of the *b*- and *y*-series ions derived from its amino acid sequence in the product ion spectrum, and the oligosaccharide moiety was deduced from the calculated molecular mass of the oligosaccharide. The heterogeneity of carbohydrate structures at 17 glycosylation sites was determined using this methodology. Our data showed that Asn2212, not previously identified as a site of glycosylation, could be glycosylated. It was also revealed that Asn158, 1341, 1350, 3309, and 3331 were occupied by high-mannose type oligosaccharides, and Asn 956, 1496, 2212, 2752, 2955, 3074, 3197, 3438, 3868, 4210, and 4404 were predominantly occupied by mono- or disialylated oligosaccharides. Asn3384, the nearest *N*-glycosylation site to the LDL-receptor binding site (amino acids 3359–3369), was occupied by a variety of oligosaccharides, including high-mannose, hybrid, and complex types. These results are useful for understanding the structure of LDL particles and oligosaccharide function in LDL-receptor ligand binding.

Key words: apolipoprotein B100/glycopeptide/liquid chromatography electrospray mass spectrometry/product ion spectrum/*N*-linked oligosaccharide

¹To whom correspondence should be addressed; e-mail:
harazono@nihs.go.jp

Introduction

Low-density lipoprotein (LDL) is the main cholesterol carrier in human plasma, and a high serum level of LDL is involved in the development of atherosclerosis. LDL is originally secreted as very low-density lipoprotein (VLDL). VLDL is converted to LDL and then removed from the circulation. Apolipoprotein B100 (apoB100) is the only protein component of LDL and is the ligand recognized by the LDL receptor. The amino acid sequence of human apoB100 has been deduced by analysis of the apoB100 cDNA sequence (Chen *et al.*, 1986; Knott *et al.*, 1986; Law *et al.*, 1986; Yang *et al.*, 1986). Mature apoB100 consists of 4536 amino acids, and its molecular weight has been calculated to be 513 kDa. ApoB100 has 19 potential *N*-glycosylation sites (Asn-X-Ser/Thr), of which 16 asparagine residues are found to be glycosylated (Yang *et al.*, 1989). The carbohydrate moieties were linked to asparagine residues at the following 16 positions: 158, 956, 1341, 1350, 1496, 2752, 2955, 3074, 3197, 3309, 3331, 3384, 3438, 3868, 4210, and 4404. The carbohydrate structures of the *N*-linked sugar chains of human apoB100 were reported to be high-mannose, hybrid, and mono- and disialylated complex type oligosaccharides (Garner *et al.*, 2001; Taniguchi *et al.*, 1979).

The role of carbohydrate moieties of apoB100 has been investigated by several laboratories. The *N*-linked oligosaccharides at the amino terminus of human apoB100 are important for the assembly and secretion of VLDL (Vukmirica *et al.*, 2002). Seven of the *N*-glycans are predicted to occur close to the LDL-receptor binding region of apoB100 and seem to have an important role (Yang *et al.*, 1986, 1989). The carbohydrate composition of apoB100, particularly sialylation, has been considered to contribute to the atherogenic properties of LDL. However, Shireman and Fisher (1979) reported that they do not appear to play a significant role in the binding of apoB100 to the LDL receptor. Furthermore, the distribution and diversity of human apoB100 oligosaccharides isolated from normolipidemic, hypercholesterolemic, and hypertriglyceridemic diabetic subjects were highly conserved even when characterized in LDL subfractions (Garner *et al.*, 2001). The potential function of apoB100 carbohydrates posthepatic secretion is not well understood. Glycoproteins have a variety of sugar chains at each glycosylation site. Because of the individual functions at each site, a comparison of glycosylation among various sites is important. Therefore, to investigate the role of carbohydrate moieties of apoB100, we attempted to determine the carbohydrate heterogeneity site-specifically.

To determine the site-specific carbohydrate heterogeneity of glycoproteins, the glycoprotein must be digested into

peptides and glycopeptides, and then both the peptide and sugar chain of each glycopeptide must be analyzed. One of the most effective techniques for mapping proteolytic fragments of glycoproteins is liquid chromatography (LC) coupled with electrospray ionization (ESI) mass spectrometry (MS) (Carr *et al.*, 1993; Duffin *et al.*, 1992; Kawasaki *et al.*, 2004; Ling *et al.*, 1991). The specific detection of glycopeptides can be achieved by monitoring specific diagnostic sugar oxonium ions, such as *m/z* 204 (HexNAc) and 366 (HexHexNAc) produced by cone voltage fragmentation, or by precursor ion scanning (Carr *et al.*, 1993; Duffin *et al.*, 1992). However, when many *N*-glycosylation sites are present within a glycoprotein, the chromatogram becomes extremely complex and assignment of the glycopeptide ions is very difficult.

We present here an alternative strategy for the site-specific glycosylation analysis of a peptide and glycopeptide mixture using LC/ESI MS/MS, where we acquired the product ion spectrum for all significant molecular ions in a data-dependent manner. Product ion spectra of molecular ions allow the specific detection of glycopeptides from a complex mixture of peptides based on the presence of diagnostic sugar oxonium ions of oligosaccharides. Furthermore, this

method allows confirmation of the amino acid sequence of a glycopeptide by the presence of b- and y-series fragment ions of the peptide. Using this method, we identified one previously unidentified *N*-glycosylated site of ApoB100 and determined the oligosaccharide heterogeneity of each of 17 *N*-glycosylation sites. Our findings provide information on the structure of apoB100 that will be useful to future studies on the structure, function, and metabolism of plasma LDL.

Results

Enzyme digestion

To determine the oligosaccharide heterogeneity at each glycosylation site, reduced and carboxymethylated apoB100 was digested into peptides and glycopeptides. Table I shows the amino acid sequences of the tryptic or chymotryptic peptides, including the putative *N*-glycosylation sites. The putative glycosylation sites were numbered (G1–19). Boldface indicates the previously reported *N*-glycosylation sites (G2–6 and G9–19). When apoB100 is digested by trypsin, potential *N*-glycosylation sites, Asn1341 (G4) and Asn1350 (G5), belong to the same peptide. Because chymotrypsin

Table I. The amino acid sequences of the tryptic or chymotryptic peptides including the putative *N*-glycosylation sites in apoB100

<i>N</i> -glycosylation site ^a		Tryptic digests	Theoretical mass ^b	Chymotryptic digests	Theoretical mass ^b
Residue	ID	Sequence		Sequence	
Asn ⁷	G1	EEEMLEN ⁷ VSLV ⁷ CPK	1677.8	EN ⁷ VSL	560.3
Asn ¹⁵⁸	G2	QVLFLDVTYGN ¹⁵⁸ CSTHFTVK	2229.1	GN ¹⁵⁸ CSTHF	822.3
Asn ⁹⁵⁶	G3	QVFPGLNYCTSGAYSN ⁹⁵⁶ ASSTDSASYPLTGDTR	3550.5	SN ⁹⁵⁶ ASSTDSASY	1088.4
Asn ¹³⁴¹	G4	LYQLQVPLLGVLDLSTNVYSNLN ¹³⁴¹	4692.3	N ¹³⁴¹ W	318.1
Asn ¹³⁵⁰	G5	WSASYSGGN ¹³⁵⁰ TSTDHFSLR	4692.3	SGGN ¹³⁵⁰ TSTDHF	1021.4
Asn ¹⁴⁹⁶	G6	FN ¹⁴⁹⁶ SSYLQGTNQITGR	1684.8	N ¹⁴⁹⁶ SSY	469.2
Asn ²²¹²	G7	TIHDLHLFIENIDFN ²²¹² K	1968.0	N ²²¹² KSGSSTASW	1023.5
Asn ²⁵³³	G8	N ²⁵³³ LTDFAEQSIQDWAK	1928.9	AAKN ²⁵³³ L	515.3
Asn ²⁷⁵²	G9	IQSPLFTLDANADIGN ²⁷⁵² GTTSANEAGIAASITAK	3231.6	DANADIGN ²⁷⁵² GTTSANEAGIAASITAKGESKL	2846.4
Asn ²⁹⁵⁵	G10	VNQNLVYESGSLN ²⁹⁵⁵ FSK	1797.9	N ²⁹⁵⁵ F	279.1
Asn ³⁰⁷⁴	G11	YNQN ³⁰⁷⁴ FSAGNNENIMEAHVINGEANLD FLNIPLTIPEMR	4359.1	NQN ³⁰⁷⁴ F	521.2
Asn ³¹⁹⁷	G12	SYN ³¹⁹⁷ ETK	740.3	N ³¹⁹⁷ ETKIKF	878.5
Asn ³³⁰⁹	G13	ELCTISHIFIPAMGN ³³⁰⁹ ITYDFFSK	2704.3	IPAMGN ³³⁰⁹ ITY	978.5
Asn ³³³¹	G14	SSVITLNTNAELFN ³³³¹ QSDIVAHLSSSSVIDALQYK	3864.0	N ³³³¹ QSDIVAHL	995.5
Asn ³³⁸⁴	G15	FVEGSHN ³³⁸⁴ STVSLTTK	1605.8	VEGSHN ³³⁸⁴ STVSL	1128.5
Asn ³⁴³⁸	G16	YDFN ³⁴³⁸ SSMLYSTAK	1525.7	N ³⁴³⁸ SSML	550.2
Asn ³⁸⁶⁸	G17	FEVDSPVYN ³⁸⁶⁸ ATWSASLK	1912.9	N ³⁸⁶⁸ ATW	490.2
Asn ⁴²¹⁰	G18	VHN ⁴²¹⁰ GSEILFSYFQDLVITLPPFLR	2836.5	SKVHN ⁴²¹⁰ GSEIL	1082.6
Asn ⁴⁴⁰⁴	G19	DFHSEYIVSASN ⁴⁴⁰⁴ FTSQLSSQVEQFLHR	3155.5	IVSASN ⁴⁴⁰⁴ F	736.4

Human apoB100 amino acid sequence (NP_000375, apolipoprotein B [gi:4502153]) was obtained from the NCBI database (www.ncbi.nlm.nih.gov/pubmed). Boldface indicates previously reported *N*-glycosylation sites. Cystein residue was carboxymethylated, and carboxymethylated cystein was underscored.

^aPotential *N*-glycosylation sites were identified with the consensus sequence NXS/T, where X is any amino acid except P.

^bMonoisotopic mass value.

can cleave apoB100 into glycopeptides containing one glycosylation site, we attempted to analyze both proteolytic fragments from trypsin digestion and chymotrypsin digestion to identify the site-specific glycosylation.

LC/ESI MS/MS analysis of tryptic digest of apoB100

The schema of a site-specific glycosylation analysis of apoB100 is shown in Figure 1. A mixture of peptides and glycopeptides was subjected to LC/ESI MS/MS with a reversed-phase column. Figure 2A shows a total ion chromatogram (TIC) of a time-of-flight (TOF) MS scan for the full scan m/z 1000–2000. When double or higher charged molecular ions were detected, the product ion spectrum was automatically acquired. Figure 2B shows a TIC of the product ion scan. The collision energy at the second quadrupole for the product ion scan was adjusted from 50 to 80 eV depending on the size and charge of the precursor ion. Under these conditions, peptide precursor ions produced b- and y-series fragment ions derived from its amino acid sequence (data not shown), and glycopeptide precursor ions produced abundant carbohydrate-specific ions, m/z 204, 186, 168, and 366 (described later). The intensity of ions at m/z 204.05–204.15 (HexNAc, 204.08) in each product ion scan are illustrated in Figure 2C. The extracted ion chromatogram at m/z 204 (Figure 2C) and 366 (data not shown) provides useful information on the selection of glycopeptide precursor ions. The product ion spectra of glycopeptides show a very characteristic pattern (see later figures). There were intense oligosaccharide-derived peaks of m/z 204 (HexNAc), 366 (HexHexNAc), 186 (HexNAc-H₂O), and 168 (HexNAc-2H₂O), and if present, 163 (Hex), 292 (Neu5Ac), and 274 (Neu5Ac-H₂O). Therefore, we can very easily distinguish the glycopeptide precursor ions from peptide ions. As expected, many parent ions having 204 and

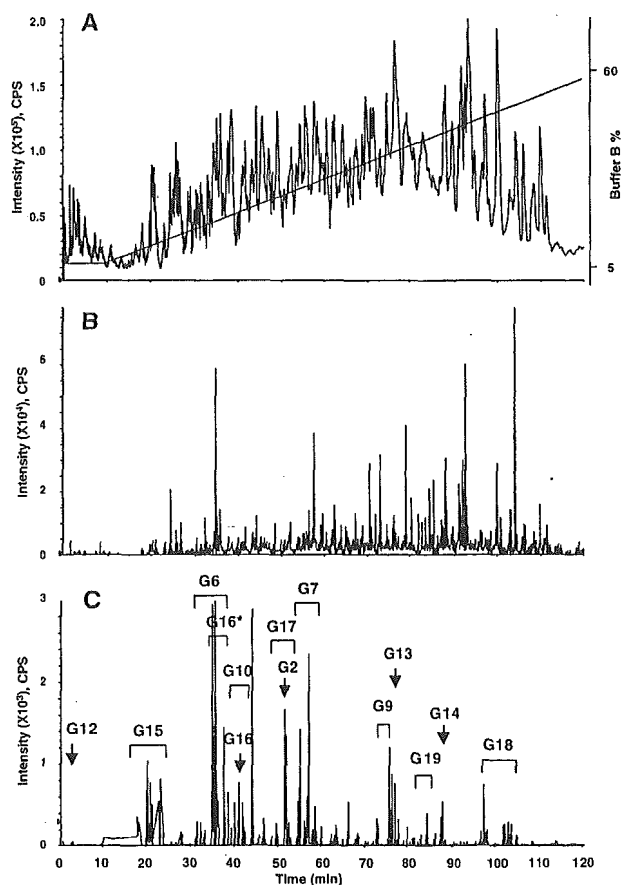


Fig. 2. LC/ESI MS/MS of tryptic digest of apolipoprotein B100. TIC of the TOF MS scan for the full scan m/z 1000–2000 and the HPLC gradient are indicated (A). TIC of the product ion scan data-dependently acquired (B). Extract ion chromatogram at m/z 204 of product ion spectra (C). Arrows and brackets denote glycopeptide fraction and *N*-glycosylation site ID. G16* was found to be oxidized at a methionine residue.

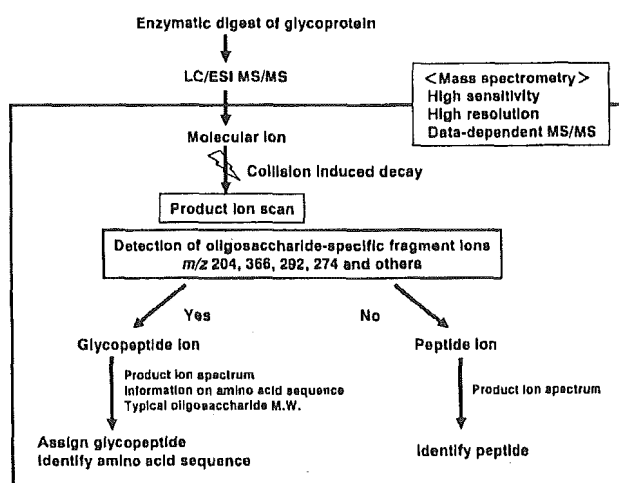


Fig. 1. Schema of site-specific glycosylation analysis. Glycoprotein was digested into peptides and glycopeptides containing only one glycosylation site. Only LC/ESI MS/MS was used. Data-dependent MS/MS acquisition was used to differentiate glycopeptide ions from peptide ions and identify the amino acid sequence of the glycopeptides. The oligosaccharide structure was deduced based on the calculated oligosaccharide molecular weight.

366 fragment ions in the product ion spectrum were detected, and most of these precursor ions were found as glycopeptides.

The glycopeptides were assigned based on an examination of product ion spectra using the information on the peptides containing a putative *N*-glycosylation site. Figures 3A, 3B, and 3C show the product ion spectra of 1412.1 (+2) at 18 min, 1160.4 (+3) at 20 min and 1271.1 (+3) at 22 min for the glycopeptides. There were intense carbohydrate B⁺ ions such as m/z 204 (HexNAc), 366 (HexHexNAc), and 186 (HexNAc-H₂O) and other weak peaks in the product ion spectra. These product ion spectra were very similar to each other (Figure 3A, 3B, and 3C). Careful examination of these product ion spectra for the glycopeptides revealed that several fragment ions were consistent with b- and y-series fragment ions derived from the peptide FVEGSHNSTVSLTTK (residue 3378–3392). The deduced b- and y-series fragment ions of the peptide FVEGSHNSTVSLTTK were listed, and the fragment ions detected in the product ion spectrum of 1160.4 (+3) are underscored in the table (Figure 3D). The molecular ions of the peptide (m/z 1606) and

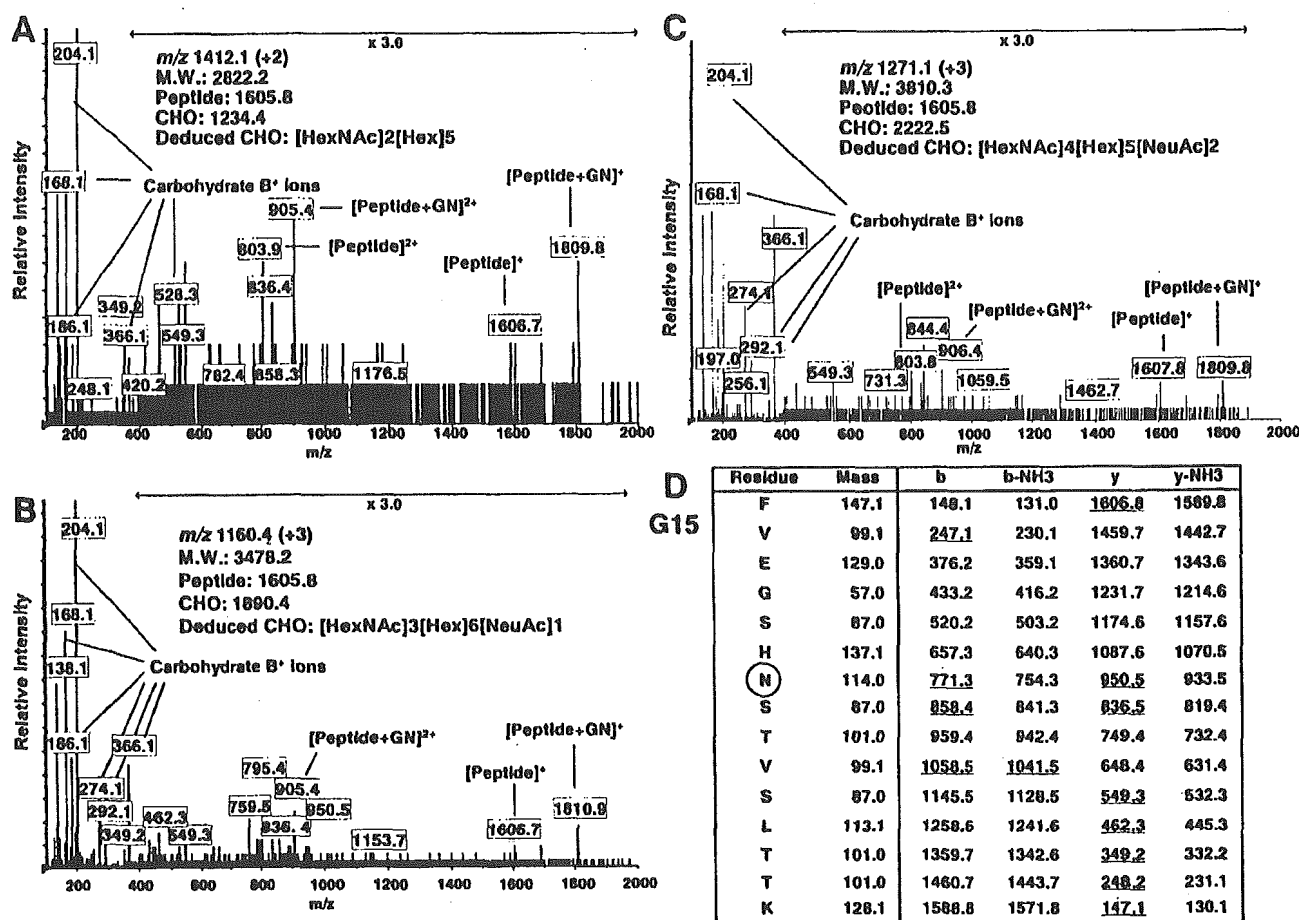


Fig. 3. Product ion spectra of the *N*-glycosylated peptides containing Asn3384 (G15). Product ion scan of m/z 1412.1 (+2) (A), 1160.4 (+3) (B), and 1271.1 (+3) (C) at 18, 20, and 22 min, respectively. These spectra show a characteristic fragmentation pattern with abundant carbohydrate-diagnostic oxonium ions at 163, 168, 186, 204, and 366 and very similar patterns to each other. The oxonium ions at m/z 292 (Neu5Ac) and 274 (Neu5Ac-H₂O) were observed in the peptides having sialylated oligosaccharide (B) and (C). Several fragment ions are consistent with the b- and y-series fragment ions derived from the peptide FVEGSHNSTVSLTTK (residue 3378–3392). [Peptide]⁺ and [peptide+GlcNAc]⁺ ions were also detected. (D) shows m/z of the proposed b- and y-series fragment ions of the peptide and the fragment ions detected in Figure 3B are underscored. Based on the calculated oligosaccharide mass, the deduced oligosaccharide structure was presented. GN, *N*-acetylglucosamine.

peptide + GlcNAc (m/z 1809) were also detected in the product ion spectra (Figure 3A, 3B, and 3C). These results suggest that these glycopeptides have the same peptide, FVEGSHNSTVSLTTK, including the *N*-glycosylation site Asn3384 (G15). Carbohydrate molecular weight was calculated by subtracting the theoretical molecular weight of the peptide (1605.8) from the calculated molecular weight of the glycopeptide and adding the molecular weight of H₂O (18.0). The oligosaccharide structure was deduced based on the molecular weight and previously reported oligosaccharides of apoB100. The presence of product ions at m/z 274 (Neu5Ac-H₂O) and 292 (Neu5Ac) suggested that those at m/z 1160.4 (+3) and 1271.1 (+3) were glycopeptide ions having sialylated oligosaccharides. Thus the carbohydrate compositions, [HexNAc]₂[Hex]₅, [HexNAc]₃[Hex]₆[Neu5Ac]₁, and [HexNAc]₄[Hex]₅[Neu5Ac]₂, were deduced from the carbohydrate molecular weights, 1234.4, 1890.4, and 2222.5, respectively.

Figures 4 shows the product ion spectra of 1294.8 (+3) at 55 min and 1152.7 (+3) at 35 min for other glycopeptides. There are intense carbohydrate B⁺ ions in the product ion spectra. Several ions consisting of b- and y-series fragment ions from the peptide TIHDLHLFIENIDHNK (residue 2198–2213) were found in the product ion spectrum of 1294.8 (+3) (Figure 4A), and detected ions are underscored in the table. The molecular ions of the peptide (m/z 1968.9) were also detected in the product ion spectra. The carbohydrate molecular weight was calculated from the molecular weight of the peptide, 1968.0, and the molecular weight of the glycopeptide, 3881.4. Carbohydrate composition was deduced from the carbohydrate molecular weight (1931.4) and presence of Neu5Ac. Thus, the peptide moiety TIHDLHLFIENIDHNK and carbohydrate composition [HexNAc]₄[Hex]₅[Neu5Ac]₁ were suggested.

Many ions in the product ion spectrum of 1152.7 (+3) were consistent with the b- and y-series fragment ions

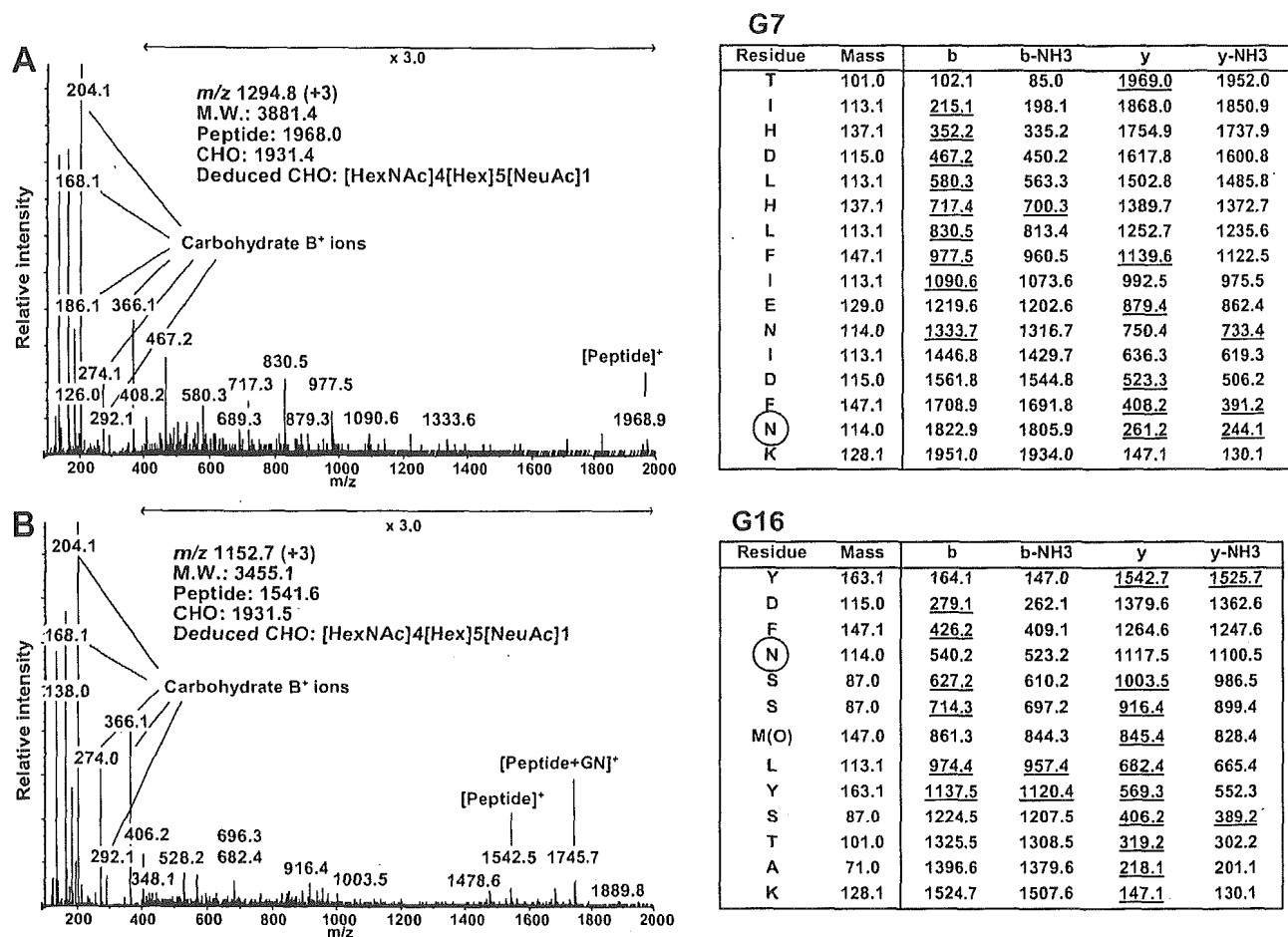


Fig. 4. Product ion spectra of the tryptic *N*-glycosylated peptides of apoB100. (A) Product ion spectrum of *m/z* 1294.8 (+3) at 55 min for the glycopeptide containing Asn2212 (G7). Several ions are consistent with the *b*- and *y*-series fragment ions derived from the peptide TIHDLHLFIENIDFNK (residue 2198–2213). Table shows *m/z* of the proposed *b*- and *y*-series fragment ions and the detected ions are underscored. (B) Product ion spectrum of *m/z* 1152.7 (+3) at 35 min for the glycopeptide containing Asn3438 (G16) with oxidized methionine. The methionine residue at 3441 was considered oxidized. Several ions are consistent with the *b*- and *y*-series fragment ions derived from the peptide YDFNSSM(O)LYSTAK (residue 3435–3447). Table shows *m/z* of the proposed *b*- and *y*-series fragment ions and the detected ions are underscored. M(O), oxidized methionine.

derived from the peptide YSFNSSMLYSTAK (Figure 4B). However, the deduced peptide ion *m/z* at 1526.7 and peptide + GlcNAc at 1729.8 were not detected. The difference of 203 between the product ions at *m/z* 1542.5 and 1745.7 suggests that the molecular weight of the peptide moiety may be 1541.5, and an increase in mass of 16 Da suggests that the methionine residue of YSFNSSMLYSTAK (residue 3435–3447, molecular weight 1525.7) was oxidized. The deduced *b*- and *y*-series fragment ions of the peptide, YSFNSSMLYSTAK, with the oxidized methionine are listed and detected peptide fragment ions are underscored. Thus, the product ions at *m/z* 1542.5 and 1745.7 were considered the peptide and peptide + GlcNAc ions, respectively. Our method identified unexpected oxidation of methionine residue (Figure 4B). The carbohydrate molecular weight was calculated, and the carbohydrate composition, [HexNAc]₄[Hex]₅[Neu5Ac]₁, was deduced from the carbohydrate molecular weight, 1931.4, and presence of Neu5Ac.

Results of site-specific glycosylation analysis from tryptic digest are summarized in Table II. To avoid misassignment, only ions that were confirmed as glycopeptides by the product ion spectra or coeluting ions with glycopeptides were listed. We determined 13 of the 19 potential *N*-glycosylation sites and the oligosaccharide heterogeneity at each site in a site-specific glycosylation analysis of the tryptic digest of apoB100. The type of oligosaccharide was deduced based on the oligosaccharide composition. Glycopeptides containing *N*-glycosylation sites Asn7, 956, 1341, 1350, 2533, and 3074 (G1, 3, 4, 5, 8, and 11) could not be detected. The relative peak intensity does not accurately express the relative amount of glycoforms, because of the different ionization efficiency of each glycoform, different detection sensitivity at *m/z*, and simultaneous acquisition of MS and MS/MS spectra. However, the relative peak intensity of each glycopeptide would provide an indication of the distribution in glycoforms.

Table II. Site-specific glycosylation analysis of the tryptic digest of apoB100 using LC/ESI-MS/MS

Glycosylation site ID	Retention time (min)	Peptide theoretical MW ^a	<i>m/z</i>	Glycopeptides			Oligosaccharide			Deduced Type ^c
				Charge	Calculated MW ^a	Calculated MW ^a	Theoretical MW ^a	Relative peak intensity (%) ^b	Composition ^c	
G1	—	1677.8	—	—	—	—	—	—	—	—
G2	51	2229.1	1365.6	+3	4093.8	1882.7	1882.6	7	[HexNAc]2[Hex]9	High mannose
	51	2229.1	1311.6	+3	3931.7	1720.6	1720.6	13	[HexNAc]2[Hex]8	High mannose
	51	2229.1	1257.5	+3	3769.5	1558.4	1558.5	22	[HexNAc]2[Hex]7	High mannose
	51	2229.1	1203.5	+3	3607.6	1396.6	1396.5	13	[HexNAc]2[Hex]6	High mannose
	51	2229.1	1149.5	+3	3445.5	1234.4	1234.4	100	[HexNAc]2[Hex]5	High mannose
	51	2229.1	1723.7	+2	3445.4	1234.4	—	—	—	—
G3	—	3550.5	—	—	—	—	—	—	—	—
G4, G5	—	4692.3	—	—	—	—	—	—	—	—
G6	33	1684.8	1451.6	+2	2901.2	1234.4	1234.4	15	[HexNAc]2[Hex]5	High mannose
	34	1684.8	1200.4	+3	3598.2	1931.4	1931.7	100	[HexNAc]4[Hex]5[Neu5Ac]1	Biantennary complex
	34	1684.8	1800.1	+2	3598.2	1931.4	—	—	—	—
	35	1684.8	1146.4	+3	3436.2	1769.4	1769.6	23	[HexNAc]4[Hex]4[Neu5Ac]1	Biantennary complex
	35	1684.8	1719.2	+2	3436.4	1769.6	—	—	—	—
	35	1684.8	1078.7	+3	3233.1	1566.3	1566.6	11	[HexNAc]3[Hex]4[Neu5Ac]1	Monoantennary complex
	35	1684.8	1132.8	+3	3395.4	1728.6	1728.6	5	[HexNAc]3[Hex]5[Neu5Ac]1	Hybrid
	35	1684.8	1186.8	+3	3557.4	1890.6	1890.7	3	[HexNAc]3[Hex]6[Neu5Ac]1	Hybrid
	35	1684.8	1240.8	+3	3719.4	2052.6	2052.7	3	[HexNAc]3[Hex]7[Neu5Ac]1	Hybrid
	37	1684.8	1297.4	+3	3889.2	2222.4	2222.8	24	[HexNAc]4[Hex]5[Neu5Ac]2	Biantennary complex
	37	1684.8	1945.7	+2	3889.4	2222.6	—	—	—	—
G7	54	1968.0	1294.8	+3	3881.4	1931.4	1931.7	66	[HexNAc]4[Hex]5[Neu5Ac]1	Biantennary complex
	58	1968.0	1044.2	+4	4172.8	2222.8	2222.8	100	[HexNAc]4[Hex]5[Neu5Ac]2	Biantennary complex
	58	1968.0	1391.9	+3	4172.7	2222.7	—	—	—	—
G8	—	1928.9	—	—	—	—	—	—	—	—
G9	73	3231.6	1360.4	+4	5437.6	2224.0	2222.8	—	[HexNAc]4[Hex]5[Neu5Ac]2	Biantennary complex
G10	40	1797.9	1238.1	+3	3711.3	1931.4	1931.7	41	[HexNAc]4[Hex]5[Neu5Ac]1	Biantennary complex
	41	1797.9	1856.7	+2	3711.4	1931.5	—	—	—	—

Table II. continued

Glycosylation site ID	Retention time (min)	Peptide theoretical MW ^a	Glycopeptides			Oligosaccharide			Relative peak intensity (%) ^b	Composition ^c	Deduced Type ^e
			m/z	Charge	Calculated MW ^a	Calculated MW ^a	Theoretical MW ^a				
G11	43	1797.9	1001.6	+4	4002.4	2222.5	2222.8	100	[HexNAc]4[Hex]5[Neu5Ac]2	Biantennary complex	
	43	1797.9	1335.1	+3	4002.3	2222.4	—	—	—	—	
	—	4359.1	—	—	—	—	—	—	—	—	
G12	2	740.3	1473.6	+2	2945.2	2222.9	2222.8	—	[HexNAc]4[Hex]5[Neu5Ac]2	Biantennary complex	
G13	75	2704.3	1102.7	+4	4406.8	1720.5	1720.6	22	[HexNAc]2[Hex]8	High mannose	
	75	2704.3	1470.0	+3	4406.9	1720.6	1558.5	54	[HexNAc]2[Hex]7	High mannose	
G14	76	2704.3	1062.2	+4	4244.8	1558.5	1558.4	—	—	—	
	76	2704.3	1415.9	+3	4244.7	1558.4	1396.5	100	[HexNAc]2[Hex]6	High mannose	
	76	2704.3	1021.6	+4	4082.4	1396.1	1234.4	50	[HexNAc]2[Hex]5	High mannose	
	76	2704.3	1361.9	+3	4082.7	1396.4	1882.6	—	[HexNAc]2[Hex]9	High mannose	
	76	2704.3	1307.9	+3	3920.7	1234.4	1599.6	8	[HexNAc]3[Hex]6	Hybrid	
	88	3864.0	1146.7	+5	5728.7	1882.7	1640.6	20	[HexNAc]4[Hex]5	Biantennary complex	
	88	3864.0	1433.1	+4	5728.3	1882.3	1437.5	20	[HexNAc]3[Hex]5	Hybrid	
	17	1605.8	1063.4	+3	3187.2	1599.4	1478.5	13	[HexNAc]4[Hex]4	Biantennary complex	
	17	1605.8	1077.0	+3	3228.0	1640.2	1234.4	4	[HexNAc]2[Hex]5	High mannose	
	17	1605.8	1009.4	+3	3025.2	1437.4	1931.7	100	[HexNAc]4[Hex]5[Neu5Ac]1	Biantennary complex	
	18	1605.8	1513.6	+2	3025.3	1437.5	1890.7	10	[HexNAc]3[Hex]6[Neu5Ac]1	Hybrid	
	18	1605.8	1023.0	+3	3066.0	1478.2	1728.6	94	[HexNAc]3[Hex]5[Neu5Ac]1	Hybrid	
18	1605.8	1412.1	+2	2822.2	1234.4	2077.7	4	[HexNAc]4[Hex]5[Neu5Ac]1[Fuc]1	Biantennary complex		
20	1605.8	1174.1	+3	3519.3	1931.5	1566.6	42	[HexNAc]3[Hex]4[Neu5Ac]1	Monoantennary complex		
20	1605.8	1760.7	+2	3519.4	1931.6	1566.6	—	—	—		
20	1605.8	1160.4	+3	3478.2	1890.4	1769.6	23	[HexNAc]4[Hex]4[Neu5Ac]1	Biantennary complex		
20	1605.8	1106.4	+3	3316.2	1728.4	2222.8	49	[HexNAc]4[Hex]5[Neu5Ac]2	Biantennary complex		
20	1605.8	1659.2	+2	3316.4	1728.6	1931.7	—	[HexNAc]4[Hex]5[Neu5Ac]1	Biantennary complex		
20	1605.8	1222.8	+3	3665.4	2077.6	1769.6	23	[HexNAc]4[Hex]4[Neu5Ac]1	Biantennary complex		
20	1605.8	1052.4	+3	3154.2	1566.4	2222.5	49	[HexNAc]4[Hex]5[Neu5Ac]2	Biantennary complex		
20	1605.8	1578.2	+2	3154.4	1566.6	1931.7	—	[HexNAc]4[Hex]5[Neu5Ac]1	Biantennary complex		
21	1605.8	1120.0	+3	3357.0	1769.2	1931.6	100	[HexNAc]4[Hex]5[Neu5Ac]1	Biantennary complex		
22	1605.8	1271.1	+3	3810.3	2222.5	1931.4	—	—	—		
G16	42	1525.7	1147.4	+3	3439.2	1931.5	1931.7	—	[HexNAc]4[Hex]5[Neu5Ac]1	Biantennary complex	
	42	1525.7	1720.7	+2	3439.3	1931.6	1931.7	—	—	—	
	35	1541.7*	1152.7	+3	3455.1	1931.4	1931.7	100	[HexNAc]4[Hex]5[Neu5Ac]1	Biantennary complex	

Table II. continued

Glycosylation site ID	Retention time (min)	Peptide theoretical MW ^a	Glycopeptides			Oligosaccharide			Deduced Type ^e	
			<i>m/z</i>	Charge	Calculated MW ^a	Calculated MW ^a	Theoretical MW ^a	Relative peak intensity (%) ^b		Composition ^c
G17	35	1541.7*	1728.6	+2	3455.2	1931.5	1769.6	9	[HexNAc]4[Hex]4[Neu5Ac]1	Biantennary complex
	36	1541.7*	1098.7	+3	3293.1	1769.4	1769.5	18	[HexNAc]3[Hex]4[Neu5Ac]1	Monoantennary complex
	36	1541.7*	1647.6	+2	3293.2	1769.5	1769.5	19	[HexNAc]4[Hex]5[Neu5Ac]2	Biantennary complex
	36	1541.7*	1546.1	+2	3090.2	1566.5	1566.6	100	[HexNAc]4[Hex]5[Neu5Ac]1	Biantennary complex
	38	1541.7*	1249.8	+3	3746.4	2222.7	2222.8	6	[HexNAc]5[Hex]6[Neu5Ac]2	Triantennary complex
	51	1912.9	1276.5	+3	3826.5	1931.6	1931.7	39	[HexNAc]4[Hex]5[Neu5Ac]2	Biantennary complex
	51	1912.9	1914.3	+2	3826.6	1931.7	1931.7	100	[HexNAc]4[Hex]5[Neu5Ac]1	Biantennary complex
	54	1912.9	1495.3	+3	4482.9	2588.0	2587.9	6	[HexNAc]5[Hex]6[Neu5Ac]2	Triantennary complex
	54	1912.9	1030.4	+4	4117.6	2222.7	2222.8	39	[HexNAc]4[Hex]5[Neu5Ac]2	Biantennary complex
	54	1912.9	1373.5	+3	4117.5	2222.6	2222.6	100	[HexNAc]4[Hex]5[Neu5Ac]1	Biantennary complex
G18	98	2836.5	1188.5	+4	4750.2	1931.7	1931.7	10	[HexNAc]4[Hex]4[Neu5Ac]1	Biantennary complex
	98	2836.5	1584.4	+3	4750.1	1931.7	1931.7	64	[HexNAc]4[Hex]5[Neu5Ac]2	Biantennary complex
	98	2836.5	1148.0	+4	4588.1	1769.6	1769.6	10	[HexNAc]4[Hex]4[Neu5Ac]1	Biantennary complex
	102	2836.5	1009.3	+5	5041.3	2222.8	2222.8	79	[HexNAc]4[Hex]5[Neu5Ac]1	Biantennary complex
G19	102	2836.5	1261.6	+4	5042.2	2223.7	2222.8	100	[HexNAc]4[Hex]5[Neu5Ac]2	Biantennary complex
	103	2836.5	1681.5	+3	5041.5	2223.0	2223.0	79	[HexNAc]4[Hex]5[Neu5Ac]1	Biantennary complex
	83	3155.5	1014.8	+5	5069.0	1931.5	1931.7	100	[HexNAc]4[Hex]5[Neu5Ac]2	Biantennary complex
	86	3155.5	1073.1	+5	5360.5	2223.0	2222.8	100	[HexNAc]4[Hex]5[Neu5Ac]2	Biantennary complex

^aMonoisotopic mass value.^bRelative peak intensity was calculated by comparing same charge state glycopeptide ions. The intensity of glycoform with maximum intensity at each glycosylation site was considered as 100%.^cThe oligosaccharide composition and type were deduced from its composition.^eThe glycopeptides including G16 were found to be oxidized at methionine residue.

When each product ion spectrum of the peptide ions in this LC/ESI MS/MS analysis was identified by the computer program Mascot, the sequence coverage of apoB100 was 38%. The ions, m/z 1177.9 (+3) at 64 min, 1289.0 (+3) at 91 min, and 1053.2 (+3) at 84 min, were identified as TIHDLHLFIENIDFN²²¹²KSGSSTASWIQNVDTK containing the potential *N*-glycosylation site Asn2212 (G7), SSVITLNTNAELFN³³³¹QSDIVAHLLSSSSVIDALQYK containing Asn3331 (G14), and DFHSEYIVSASN⁴⁴⁰⁴-FTSQLSSQVEQFLHR containing Asn4404 (G19), respectively (data not shown). These results indicate that some parts of these glycosylation sites were not glycosylated. There were many unexplained peptides and glycopeptides in the digest (data not shown). This may be due to the unexpected digestion or nonspecific cleavage of apolipoprotein B100 as well as the multiple isoforms of the proteins.

LC/ESI MS/MS analysis of chymotryptic digest of apoB100

To determine the carbohydrate at undetected glycosylation sites in the tryptic digest including Asn1341 and 1350 (G4 and G5), which belong to the same tryptic peptide, the chymotrypsin digest was analyzed by LC/ESI MS/MS using the same methodology. Figure 5A shows a TIC of the TOF MS scan for the full scan m/z 700–2000. The collision energy was adjusted at 40–80 eV depending on the precursor ions. A TIC of the product ion scan and extracted ion chromatogram at m/z 204.05–204.15 (HexNAc) are presented in Figure 5B and 5C, respectively.

Figure 6A shows the product ion spectrum of 768.4 (+2) at 14 min for the chymotryptic glycopeptide. The carbohydrate B⁺ ions, y1 and b2 ions of peptide NW (residue 1341–1342), and peptide + GlcNAc ion were found in the product ion spectrum. The carbohydrate composition, [HexNAc]₂[Hex]₅, was deduced from the calculated carbohydrate molecular ion, 1234.6. Figure 6B shows the product ion spectrum of 1444.1 (+2) at 9 min for the glycopeptide. The carbohydrate B⁺ ions, peptide and peptide + GlcNAc ions, and peptide fragment ions from the peptide SGGNT-STDHF (residue 1347–1356) were detected in the product ion spectrum. Carbohydrate molecular weight, 1882.8, was calculated and the oligosaccharide composition, [HexNAc]₂[Hex]₆, was deduced from the molecular weight. The peptide fragment ions were also detected in the product ion spectrum for the chymotryptic glycopeptides as tryptic glycopeptides. The peptide and peptide + GlcNAc ions were detected in product ion spectra. These ions helped us determine the peptide moiety of the glycopeptide ion.

Results of the site-specific analysis of glycosylation of the chymotryptic digest are summarized in Table III. The oligosaccharide heterogeneity at each of 13 *N*-glycosylation sites was determined by LC/ESI MS/MS from the chymotryptic digest of apoB100 (Table III).

Carbohydrate diversity of each site

Results for the tryptic digest and chymotryptic digest of apoB100 are listed in Table IV. The oligosaccharide composition and type were deduced based on the molecular weight and previously reported oligosaccharide structures of apoB100. No information on glycosylation at Asn7 and 2533 (G1 and 8) was obtained from the analysis of the

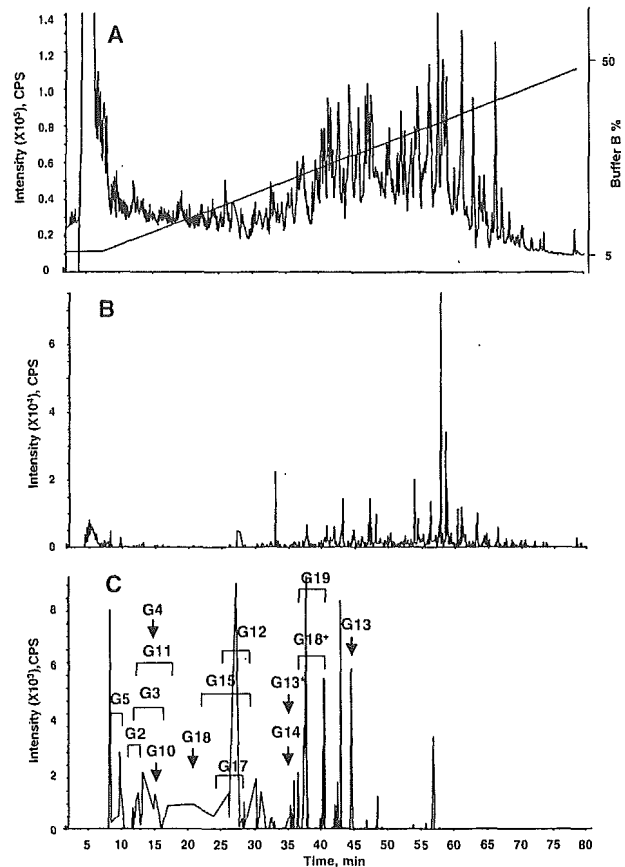


Fig. 5. LC/ESI MS/MS of chymotryptic digest of apolipoprotein B100. TIC of TOF MS scan for the full scan m/z 700–2000 and the HPLC gradient are indicated (A). TIC of the product ion scan data-dependently acquired (B). Extract ion chromatogram at m/z 204 of product ion spectra (C). Arrows and brackets denote glycopeptide fraction and *N*-glycosylation site ID. G13* was found to be oxidized at a methionine residue. G18* was found as missed cleaved glycopeptides.

tryptic or chymotryptic digest. When the tryptic digest of apoB100 was analyzed by LC/ESI MS/MS with the MS range m/z 400–2000, the sequence coverage of apoB100 was 41% and tryptic peptides containing Asn7, 2212, 2533, or 2955 (G1, 7, 8, or 10) were detected (data not shown). Together with the result of LC/ESI MS/MS with the MS range m/z 1000–2000, Asn7 and 2533 (G1 and 8) were not glycosylated or glycosylated only under detection sensitivity, and Asn2212, 2955, 3331, and 4404 (G7, 10, 14, and 19) were partially glycosylated. These findings indicate that 17 of 19 potential *N*-glycosylation sites in apoB100 were glycosylated.

The most heterogeneous oligosaccharides were found at Asn3384 (G15). Asn3384 possessed neutral or monosialylated hybrid and monoantennary complex type and mono- or disialylated biantennary complex type oligosaccharides as well as one high-mannose type oligosaccharide. Asn158, 1341, 1350, 3309, and 3331 (G2, 4, 5, 13, and 14) were occupied by high-mannose type oligosaccharides, whereas Asn956, 1496, 2212, 2752, 2955, 3074, 3197, 3438, 3868,

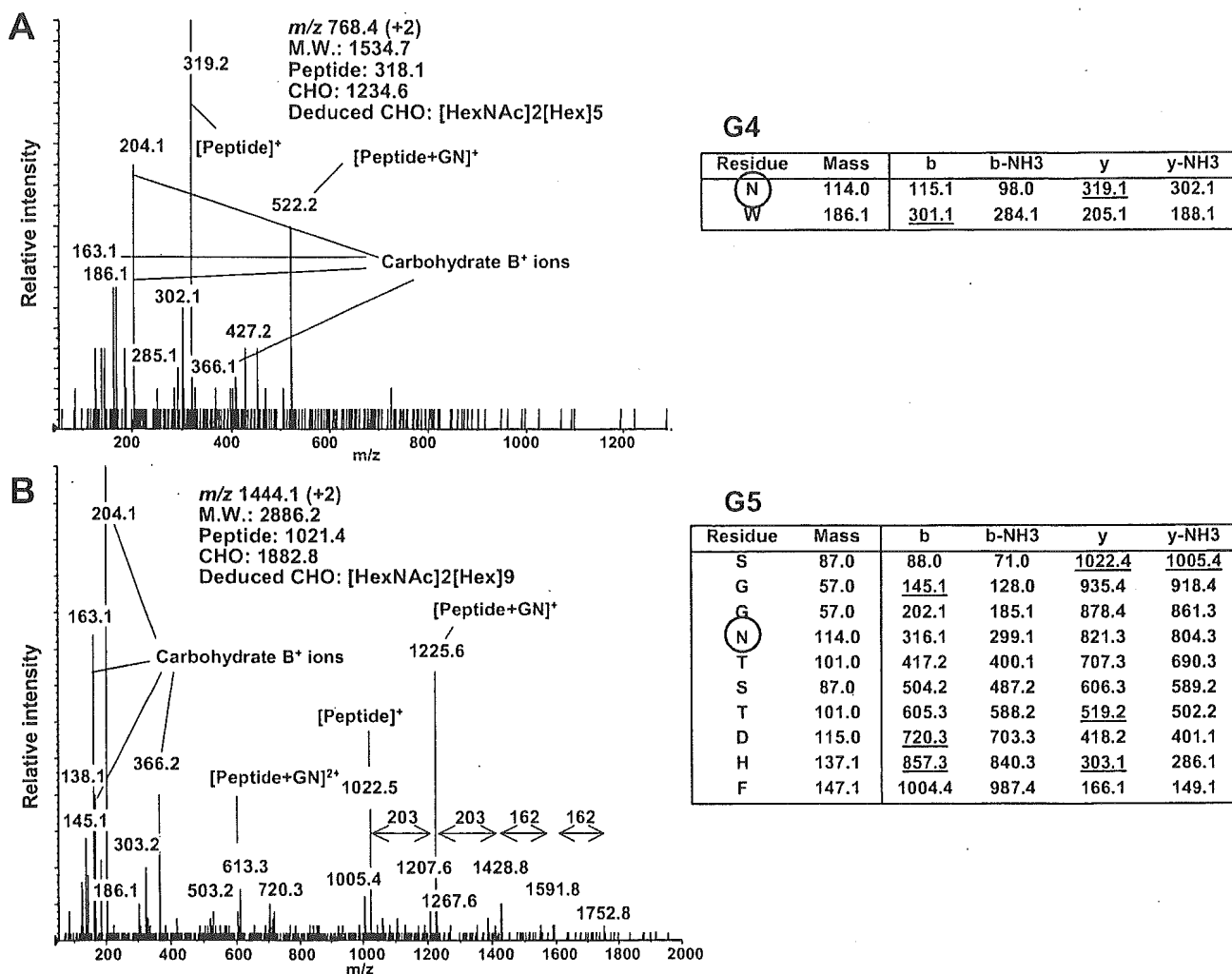


Fig. 6. Product ion spectra of the chymotryptic *N*-glycosylated peptides of apoB100. (A) Product ion spectrum of m/z 768.4 (+2) at 14 min for the glycopeptide consisting of residues 1341–1342. Peptide b and y ions of the peptide NW were found. Table shows m/z of the proposed b- and y-series fragment ions, and the detected ions are underscored. (B) Product ion spectrum of m/z 1444.1 (+2) at 9 min for the glycopeptide consisting of residues 1347–1356. Several ions are consistent with the b- and y-series fragment ions derived from the peptide SGGNTSTDHF. Table shows m/z of the proposed b- and y-series fragment ions, and the detected ions are underscored.

4210, and 4404 (G3, 6, 7, 9–12, and 16–19) were predominantly occupied by monosialylated or disialylated biantennary complex type oligosaccharides (Figure 7).

Discussion

Although the role of the carbohydrate structures in LDL and/or apoB100 has been examined in several studies (Attie *et al.*, 1979; Filipovic *et al.*, 1979; Fujioka *et al.*, 2000; Orekhov *et al.*, 1989; Shireman and Fisher, 1979), it is still unknown. It is necessary to elucidate the diversity of the oligosaccharides at each *N*-glycosylation site. This is the first report on the characterization of *N*-linked oligosaccharides in apoB100 at each glycosylation site. The protein was initially carboxymethylated and digested with an enzyme

(trypsin or chymotrypsin), and then the complex mixtures of peptides and glycopeptides were subjected to LC/ESI MS/MS analysis. Product ion scan of each precursor ion was carried out in a data-dependent manner. The glycopeptide molecular ions were easily distinguished from peptide ions by the presence of carbohydrate-related oxonium ions, such as m/z 204 (HexNAc), 186 (HexNAc–H₂O), 168 (HexNAc–H₂O), 366 (HexHexNAc), and others in product ion spectra. Furthermore, product ion spectra provided information for the elucidation of the amino acid sequence of the glycopeptides.

The oligosaccharide structure could be deduced based on the calculated molecular weight of the oligosaccharide moiety. The glycopeptide precursor ion was assigned using three strategies. (1) By comparing the product ions of the glycopeptide with the expected fragment ions derived from

Table III. Site-specific glycosylation analysis of the chymotryptic digest of apoB100 using LC/ESI MS/MS

Glycosylation site ID	Retention time (min)	Peptide theoretical MW ^a	Glycopeptides			Oligosaccharide			Deduced Type ^c	
			m/z	Charge	Calculated MW ^a	Calculated MW ^a	Theoretical MW ^a	Relative peak intensity (%) ^b		Composition ^c
G1	—	560.3	—	—	—	—	—	—	—	
G2	11	822.3	1344.5	+2	2687.0	1882.7	1882.6	4	[HexNAc]2[Hex]9	High mannose
	11	822.3	1263.5	+2	2525.0	1720.7	1720.6	7	[HexNAc]2[Hex]8	High mannose
	11	822.3	1182.5	+2	2363.0	1558.7	1558.5	15	[HexNAc]2[Hex]7	High mannose
	12	822.3	1101.4	+2	2200.8	1396.5	1396.5	12	[HexNAc]2[Hex]6	High mannose
	12	822.3	1020.4	+2	2038.8	1234.5	1234.4	100	[HexNAc]2[Hex]5	High mannose
G3	12	1088.4	1001.8	+3	3002.4	1932.0	1931.7	70	[HexNAc]4[Hex]5[Neu5Ac]1	Biantennary complex
	15	1088.4	1098.8	+3	3293.4	2223.0	2222.8	100	[HexNAc]4[Hex]5[Neu5Ac]2	Biantennary complex
G4	14	318.1	768.4	+2	1534.8	1234.7	1234.4	—	[HexNAc]2[Hex]5	High mannose
G5	9	1021.4	963.1	+3	2886.3	1882.9	1882.6	100	[HexNAc]2[Hex]9	High mannose
	9	1021.4	1444.1	+2	2886.2	1882.8	—	—	—	—
	9	1021.4	1363.1	+2	2724.2	1720.8	1720.6	40	[HexNAc]2[Hex]8	High mannose
	9 ^d	1021.4	1282.1	+2	2562.2	1558.8	1558.5	16	[HexNAc]2[Hex]7	High mannose
G6	—	469.2	—	—	—	—	—	—	—	—
G7	—	1023.5	—	—	—	—	—	—	—	—
G8	—	515.3	—	—	—	—	—	—	—	—
G9	—	2846.4	—	—	—	—	—	—	—	—
G10	15	279.1	829.0	+3	2484.1	2223.0	2222.8	—	[HexNAc]4[Hex]5[Neu5Ac]2	Biantennary complex
	15	279.1	1243.0	+2	2484.0	2222.9	—	—	—	—
G11	13	521.2	812.7	+3	2435.1	1931.9	1931.7	100	[HexNAc]4[Hex]5[Neu5Ac]1	Biantennary complex
	13	521.2	1218.5	+2	2435.0	1931.8	—	—	—	—
	16	521.2	909.8	+3	2726.3	2223.0	2222.8	52	[HexNAc]4[Hex]5[Neu5Ac]2	Biantennary complex
G12	28	878.5	1028.8	+3	3083.4	2222.9	2222.8	—	[HexNAc]4[Hex]5[Neu5Ac]2	Biantennary complex
G13	44	978.5	1341.6	+2	2681.2	1720.7	1720.6	31	[HexNAc]2[Hex]8	High mannose
	44	978.5	1260.6	+2	2519.1	1558.6	1558.5	50	[HexNAc]2[Hex]7	High mannose
	44	978.5	1179.5	+2	2357.1	1396.6	1396.5	100	[HexNAc]2[Hex]6	High mannose

Table III. continued

Glycosylation site ID	Retention time (min)	Peptide theoretical MW ^a	Glycopeptides			Oligosaccharide			Relative peak intensity (%) ^b	Composition ^c	Deduced Type ^e
			m/z	Charge	Calculated MW ^a	Calculated MW ^a	Theoretical MW ^a				
G14	44	978.5	1098.5	2	2195.0	1234.5	1234.4	75	[HexNAc]2[Hex]5	High mannose	
	35 ^d	995.5*	1349.6	+2	2697.1	1719.6	1720.6	16	[HexNAc]2[Hex]8	High mannose	
	35 ^d	995.5*	1268.5	+2	2535.0	1557.5	1558.5	49	[HexNAc]2[Hex]7	High mannose	
	35	995.5*	1187.5	+2	2373.0	1395.5	1396.5	100	[HexNAc]2[Hex]6	High mannose	
	35	995.5*	1106.5	+2	2211.0	1233.5	1234.4	89	[HexNAc]2[Hex]5	High mannose	
G15	35	995.5	954.4	+3	2860.3	1882.8	1882.6	—	[HexNAc]2[Hex]9	High mannose	
	35	995.5	1431.2	+2	2860.3	1882.8	—	—	—	—	
	24	1128.5	1173.5	+2	2345.0	1234.6	1234.4	3	[HexNAc]2[Hex]5	High mannose	
	24 ^d	1128.5	1275.0	+2	2548.0	1437.5	1437.5	9	[HexNAc]3[Hex]5	Hybrid	
	27	1128.5	1015.1	+3	3042.4	1931.9	1931.7	100	[HexNAc]4[Hex]5[Neu5Ac]1	Biantennary complex	
G16	27	1128.5	947.4	+3	2839.3	1728.8	1728.6	79	[HexNAc]3[Hex]5[Neu5Ac]1	Hybrid	
	27	1128.5	893.4	+3	2677.3	1566.8	1566.6	23	[HexNAc]3[Hex]4[Neu5Ac]1	Monoantennary complex	
	30	1128.5	1112.2	+3	3333.5	2223.0	2222.8	28	[HexNAc]4[Hex]5[Neu5Ac]2	Biantennary complex	
	—	550.2	—	—	—	—	—	—	—	—	
	28	490.2	899.4	+3	2695.2	2223.0	2222.8	—	[HexNAc]4[Hex]5[Neu5Ac]2	Biantennary complex	
G17	28	490.2	1348.5	+2	2695.0	2222.8	—	—	—	—	
	21	1082.6	999.8	+3	2996.4	1931.8	1931.7	100	[HexNAc]4[Hex]5[Neu5Ac]1	Biantennary complex	
	25	1082.6	1096.8	+3	3287.4	2222.8	2222.8	51	[HexNAc]4[Hex]5[Neu5Ac]2	Biantennary complex	
	37	1229.6 ^f	786.9	+4	3143.5	1931.9	1931.7	100	[HexNAc]4[Hex]5[Neu5Ac]1	Biantennary complex	
	37	1229.6 ^f	1048.8	+3	3143.5	1931.8	—	—	—	—	
G18	38	1229.6 ^f	994.8	+3	2981.5	1769.9	1769.6	14	[HexNAc]4[Hex]4[Neu5Ac]1	Biantennary complex	
	40	1229.6 ^f	859.7	+4	3434.6	2223.0	2222.8	67	[HexNAc]4[Hex]5[Neu5Ac]2	Biantennary complex	
	40	1229.6 ^f	1145.9	+3	3434.6	2223.0	—	—	—	—	
	37	736.4	884.4	+3	2650.3	1931.9	1931.7	100	[HexNAc]4[Hex]5[Neu5Ac]1	Biantennary complex	
	37	736.4	1326.1	+2	2650.2	1931.8	—	—	—	—	
G19	40	736.4	981.4	+3	2941.2	2222.8	2222.8	94	[HexNAc]4[Hex]5[Neu5Ac]2	Biantennary complex	

^aMonoisotopic mass value.^bRelative peak intensity was calculated by comparing same charge state glycopeptide ions. The intensity of glycoform with maximum intensity at each glycosylation site was considered as 100%.^cThe oligosaccharide composition and type were deduced from its composition.^dProduct ion spectra were not acquired. These ions were considered as glycopeptides by the mass differences of 162(Hex) or 203(HexNAc) from the glycopeptides.^eThe glycopeptides including G13 were found to be oxidized at methionine residue.^fPeptides of these glycopeptides including G18 were found as missed cleaved. The peptide sequence was considered as SKVHN²¹⁰GSEILF.

Table IV. Summary of apoB100 oligosaccharide structure obtained from tryptic digest and chymotryptic digest

Glycosylation site ID	Deduced oligosaccharide composition ^a	Deduced oligosaccharide type ^a
G1	Not glycosylated	—
G2	[HexNAc]2[Hex]9	High mannose
G3	[HexNAc]4[Hex]5[Neu5Ac]1	Biantennary complex
G4	[HexNAc]2[Hex]5	High mannose
G5	[HexNAc]2[Hex]9	High mannose
G6	[HexNAc]2[Hex]5	High mannose
	[HexNAc]3[Hex]7[Neu5Ac]1	Hybrid
	[HexNAc]3[Hex]4[Neu5Ac]1	Monoantennary complex
	[HexNAc]4[Hex]4[Neu5Ac]1	Biantennary complex
	[HexNAc]4[Hex]5[Neu5Ac]2	Biantennary complex
G7	[HexNAc]4[Hex]5[Neu5Ac]1	Biantennary complex
	[HexNAc]4[Hex]5[Neu5Ac]2	Biantennary complex
G8	Not glycosylated	—
G9	[HexNAc]4[Hex]5[Neu5Ac]2	Biantennary complex
G10	[HexNAc]4[Hex]5[Neu5Ac]1	Biantennary complex
G11	[HexNAc]4[Hex]5[Neu5Ac]1	Biantennary complex
G12	[HexNAc]4[Hex]5[Neu5Ac]2	Biantennary complex
G13	[HexNAc]2[Hex]8	High mannose
G14	[HexNAc]2[Hex]9	High mannose
G15	[HexNAc]2[Hex]5	High mannose
	[HexNAc]3[Hex]6	Hybrid
	[HexNAc]3[Hex]4[Neu5Ac]1	Monoantennary complex
	[HexNAc]4[Hex]4	Biantennary complex
	[HexNAc]4[Hex]5[Neu5Ac]1[Fuc]1	Biantennary complex
G16	[HexNAc]3[Hex]4[Neu5Ac]1	Biantennary complex
	[HexNAc]4[Hex]4[Neu5Ac]1	Monoantennary complex
G17	[HexNAc]4[Hex]5[Neu5Ac]1	Biantennary complex
	[HexNAc]5[Hex]6[Neu5Ac]2	Biantennary complex
G18	[HexNAc]4[Hex]4[Neu5Ac]1	Triantennary complex
	[HexNAc]4[Hex]5[Neu5Ac]2	Biantennary complex
G19	[HexNAc]4[Hex]5[Neu5Ac]1	Biantennary complex

^aThe oligosaccharide structure was deduced from the molecular weight and previously reported oligosaccharide structures of apoB100.

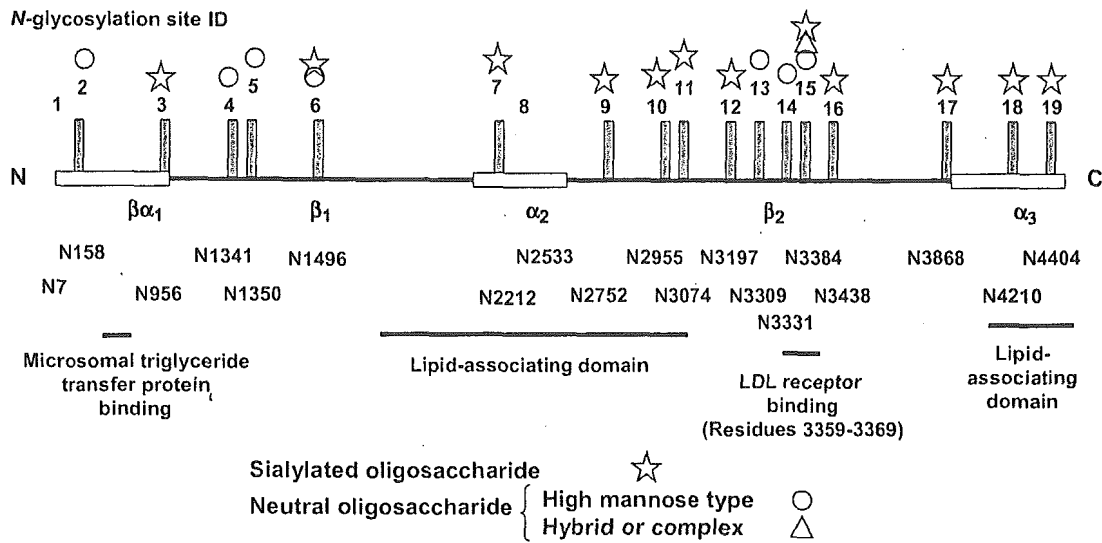


Fig. 7. *N*-glycosylation site of apoB100 and *N*-glycans at each site. *N*-glycosylation sites were shown on the pentapartite structure model, NH₂- $\beta\alpha_1$ - β_1 - α_2 - β_2 - α_3 -COOH, previously reported (Segrest *et al.*, 1994). Circle, triangle, and star indicate high-mannose type oligosaccharides, neutral hybrid or neutral complex oligosaccharides, and mono- or disialylated oligosaccharides, respectively. High-mannose type oligosaccharides were found around the *N*-terminal and near the LDL-receptor binding site, and the other sites were attached by mono- or disialylated oligosaccharides. These oligosaccharide structures may reflect the local 3D structure of VLDL/LDL and may play a biological role.

the peptide containing the *N*-linked glycosylation site, we could directly deduce the peptide moiety. The molecular weight of the oligosaccharide moiety was calculated from the observed molecular weight of the glycopeptide and the theoretical molecular weight of the identified peptide. The carbohydrate composition and structure were deduced from the calculated molecular weight of the oligosaccharide. (2) There were relatively intense peaks of the peptide and peptide + GlcNAc ions in the glycopeptide product ion spectrum. Thus the *m/z* difference of 203 between fragment ions in the product ion spectrum could suggest the molecular weight of the peptide moiety. The peptide was determined from this suggested molecular weight and the molecular weight of the peptides containing the putative *N*-glycosylation site. The molecular weight of the carbohydrate was calculated, and the carbohydrate composition and structure were deduced. (3) Possible glycopeptide masses were calculated from the peptide masses containing the *N*-linked glycosylation site and possible *N*-linked oligosaccharide masses. The possible glycopeptide mass with the measured mass of the glycopeptide was identified. Assignment of peptide moiety was confirmed by the presence of the fragment ions derived from the peptide in the product ion spectrum.

The elution time as well as mass of a glycopeptide is also helpful to elucidate the oligosaccharide structure. The glycopeptides were eluted following reversed-phase high-performance LC based on the peptide and further separated based on the structure of the attached oligosaccharide (Kawasaki *et al.*, 2004). The glycopeptides having the same amino acid sequence were eluted in order of the number of Neu5Ac. Our results show that LC/ESI MS/MS with high sensitivity and high detection resolution is a powerful technique for the site-specific glycosylation analysis of glycoprotein.

Our study revealed that 17 of the 19 potential *N*-glycosylation sites in apoB100 were glycosylated, and the diversity of oligosaccharides at each of these *N*-glycosylation sites was determined. The deduced oligosaccharide structures in the present study were consistent with the structures previously identified in apoB100 (Garner *et al.*, 2001). Asn2212, which was reported to be unglycosylated (Yang *et al.*, 1989), could be glycosylated. The *N*-glycan structures and patterns are very different at each site. Asn158, 1341, 1350, 3309, and 3331 were occupied by high-mannose type oligosaccharides. The other sites except Asn1496 and 3384 (G6 and G15) were predominantly occupied by mono- or disialylated biantennary complex type oligosaccharides, and no neutral oligosaccharides were detected. These sialylated glycans may play an important biological role. Asn1496 and 3384 were occupied by high-mannose, hybrid, and complex type *N*-linked oligosaccharides. Hybrid-type oligosaccharides were found only at these two sites. The oligosaccharides at Asn 3384 are most heterogeneous, and at least 12 different oligosaccharide structures were present. Neutral complex type and neutral hybrid type oligosaccharides were detected only at this site. It is unlikely that this oligosaccharide heterogeneity is due to the fact that the apoB100 used in this study was extracted from the pooled serum of normolipidemic subjects, because no hybrid type oligosaccharides were detected except at Asn1496 and 3384 in this study, and it was reported that the diversity of the oligosaccharides of apoB100 was highly conserved among subjects (Garner *et al.*, 2001; Taniguchi *et al.*, 1989). It may be suggested that the diversity of the oligosaccharides at each glycosylation site was also conserved among subjects.

The relationship between sialylation and LDL-receptor binding has been examined. Desialylation of LDL increased the internalization of LDL by aortic smooth muscle cells

(Filipovic *et al.*, 1979), macrophage (Fujioka *et al.*, 2000) and aortic intimal cells (Orekhov *et al.*, 1989), but had no effect on degradation in hepatocytes (Attie *et al.*, 1979). These findings appear controversial. Asn3309, 3331, and 3384 are located near the LDL-receptor binding site in apoB100 (residues 3359–3369). Our data showed that these glycosylation sites were populated by high-mannose type (at Asn3309 and 3331) or a variety of oligosaccharides, including neutral or sialylated oligosaccharides (at Asn3384). These findings may indicate that sialic acid residues of apoB100 did not play a significant role in LDL-receptor binding and that desialylated LDL might be internalized by another mechanism. Shireman and Fisher (1979) reported that the removal of carbohydrate from LDL did not alter its binding to fibroblasts. Thus the carbohydrate moieties of LDL might not have a significant role in LDL-receptor binding.

The most interesting observation was that the most heterogeneous oligosaccharides were found at the *N*-glycosylation site (Asn3384) nearest to the LDL-receptor binding site. ApoB100 enwraps the VLDL and LDL particle. The C-terminal crosses over near the LDL-receptor binding site and inhibits binding of VLDL to the LDL receptor (Boren *et al.*, 1998). Conversion of VLDL to smaller LDL allows interaction with the LDL receptor. It is likely that the size of the VLDL/LDL particle could affect the 3D conformation around here. Thus the variety of oligosaccharide at Asn3384 may reflect the local 3D conformation of the VLDL particle and accessibility of trimming and glycosyl transferase enzymes.

The procedure described in this article provides an easy and efficient method for the identification of glycosylation sites and oligosaccharide heterogeneity of glycoproteins. Site-specific glycosylation analysis of apoB100 revealed that the diversity of oligosaccharide was distinct at each site. These data provide information to understand the role of oligosaccharides of apoB100 in LDL particles

Materials and methods

Materials

Acetonitrile, formic acid, chymotrypsin, and guanidine hydrochloride were from Wako Pure Chemicals (Osaka, Japan). Tosylphenylalanine chloromethane (TPCK)-treated trypsin was from Sigma (St. Louis, MO). Human apoB100 was purchased from MP Biomedicals (Irvine, CA). This product is derived from pooled human plasma, which is not particularly high-fat plasma. The water used was obtained from a Milli-Q water system (Millipore, Bedford, MA). All other reagents were of the highest quality available.

Reduction and *S*-carboxymethylation of apoB100

ApoB100 (500 µg) was dissolved in 810 µl of 0.5 M Tris-HCl buffer (pH 8.5) that contained 8 M guanidine hydrochloride and 5 mM ethylenediamine tetra-acetic acid. After the addition of 6 µl 2-mercaptoethanol, the mixture was incubated for 2 h at 40°C. Then, 17 mg of monoiodoacetic acid was added, and the resulting mixture was incubated for 2 h at 40°C in the dark. The reaction mixture was applied to a PD-10 column (Amersham Pharmacia Biotech,

Uppsala, Sweden) to remove the reagents, and the eluate was lyophilized.

Enzyme digestion of apoB100

Reduced and carboxymethylated apoB100 was redissolved in 500 µl 0.1 M Tris-HCl buffer (pH 8.0). Half of the reduced and carboxymethylated apoB100 was incubated with 0.02 µg/µl of TPCK-treated trypsin (1:50 w/w) for 2 h at 37°C and the rest was incubated with 0.04 µg/µl of chymotrypsin (1:25 w/w) for 72 h at 37°C. The enzyme digestions were stopped by storing at -20°C before analysis.

High-performance LC of trypsin or chymotrypsin-digested apoB100

Tryptic digest (4 µg, about 8 pmol) and chymotryptic digest (2 µg, about 4 pmol) were analyzed by LC/ESI MS/MS. High-performance LC was performed on a Paradigm MS 4 equipped with a Magic C18 column (0.2 × 50 mm, Michrom BioResources, Auburn, CA). The eluents consisted of water containing 2% (v/v) acetonitrile and 0.1% (v/v) formic acid (pump A) and 90% acetonitrile and 0.1% formic acid (pump B). Trypsin- or chymotrypsin-digested samples of apoB100 were eluted with 5% B for 10 min, followed by a linear gradient from 5% to 70% of pump B in 130 min at a flow rate of 2 µl/min.

ESI Q-TOF MS/MS

MS analyses were performed using a QSTAR Pulsar i quadrupole TOF mass spectrometer (AB/MDS Sciex, Toronto, Canada) equipped with a nano-electrospray ion source. The mass spectrometer was operated in the positive ion mode. The nanospray voltage was set at 2500 V. Mass spectra for MS analysis were acquired over *m/z* 1000–2000 and 700–2000 for tryptic and chymotryptic digests, respectively, and for MS/MS analysis, over *m/z* 100–2000. After every regular MS acquisition, MS/MS acquisition was performed against multiple charged ions. The molecular ions were selected by data-dependent acquiring in the quadrupole analyzer and fragmented in the hexapole collision cell. The collision energy was varied between 40 and 80 eV depending on the size and charge of the molecular ion. All signals were monoisotopically resolved. Accumulation time of spectra is 1.0 and 2.0 s for MS and MS/MS, respectively.

Acknowledgments

We thank Dr. Nishimaki-Mogami for helpful suggestions. This study was supported by a grant-in-aid for Research on Health Sciences focusing on Drug Innovation from the Japan Health Sciences Foundation.

Abbreviations

apoB100, apolipoprotein B100; ESI, electrospray ionization; LC, liquid chromatography; LDL, low-density lipoprotein; MS, mass spectrometry; TIC, total ion chromatogram; TOF, time of flight; TPCK, Tosylphenylalanine chloromethane; VLDL, very low-density lipoprotein.

References

- Attie, A.D., Weinstein, D.B., Freeze, H.H., Pittman, R.C., and Steinberg, D. (1979) Unaltered catabolism of desialylated low-density lipoprotein in the pig and in cultured rat hepatocytes. *Biochem. J.*, **180**, 647–654.
- Boren, J., Lee, I., Zhu, W., Arnold, K., Taylor, S., and Innerarity, T.L. (1998) Identification of the low density lipoprotein receptor-binding site in apolipoprotein B100 and the modulation of its binding activity by the carboxyl terminus in familial defective apo-B100. *J. Clin. Invest.*, **101**, 1084–1093.
- Carr, S.A., Huddleston, M.J., and Bean, M.F. (1993) Selective identification and differentiation of *N*- and *O*-linked oligosaccharides in glycoproteins by liquid chromatography-mass spectrometry. *Protein Sci.*, **2**, 183–196.
- Chen, S.H., Yang, C.Y., Chen, P.F., Setzer, D., Tanimura, M., Li, W.H., Gotto, A.M. Jr. and Chan, L. (1986) The complete cDNA and amino acid sequence of human apolipoprotein B-100. *J. Biol. Chem.*, **261**, 12918–12921.
- Duffin, K.L., Welply, J.K., Huang, E., and Henion, J.D. (1992) Characterization of *N*-linked oligosaccharides by electrospray and tandem mass spectrometry. *Anal. Chem.*, **64**, 1440–1448.
- Filipovic, I., Schwarzmann, G., Mraz, W., Wiegandt, H., and Buddecke, E. (1979) Sialic-acid content of low-density lipoproteins controls their binding and uptake by cultured cells. *Eur. J. Biochem.*, **93**, 51–55.
- Fujioka, Y., Taniguchi, T., Ishikawa, Y., and Yokoyama, M. (2000) Significance of acidic sugar chains of apolipoprotein B-100 in cellular metabolism of low-density lipoproteins. *J. Lab. Clin. Med.*, **136**, 355–362.
- Garner, B., Harvey, D.J., Royle, L., Frischmann, M., Nigon, F., Chapman, M.J., and Rudd, P.M. (2001) Characterization of human apolipoprotein B100 oligosaccharides in LDL subfractions derived from normal and hyperlipidemic plasma: deficiency of alpha-*N*-acetylneuraminyl-lactosyl-ceramide in light and small dense LDL particles. *Glycobiology*, **11**, 791–802.
- Kawasaki, N., Ohta, M., Itoh, S., and Hayakawa, T. (2004) Analyses of glycopeptides and glycoproteins by liquid chromatography-mass spectrometry and liquid chromatography-tandem mass spectrometry. *Methods Mol. Biol.*, **251**, 263–274.
- Knott, T.J., Pease, R.J., Powell, L.M., Wallis, S.C., Rall, S.C. Jr. Innerarity, T.L., Blackhart, B., Taylor, W.H., Marcel, Y., Milne, R., and others. (1986) Complete protein sequence and identification of structural domains of human apolipoprotein B. *Nature*, **323**, 734–738.
- Law, S.W., Grant, S.M., Higuchi, K., Hospattankar, A., Lackner, K., Lee, N., and Brewer, H.B. Jr. (1986) Human liver apolipoprotein B-100 cDNA: complete nucleic acid and derived amino acid sequence. *Proc. Natl Acad. Sci. USA*, **83**, 8142–8146.
- Ling, V., Guzzetta, A.W., Canova-Davis, E., Stults, J.T., Hancock, W.S., Covey, T.R., and Shushan, B.I. (1991) Characterization of the tryptic map of recombinant DNA derived tissue plasminogen activator by high-performance liquid chromatography-electrospray ionization mass spectrometry. *Anal. Chem.*, **63**, 2909–2915.
- Orekhov, A.N., Tertov, V.V., Mukhin, D.N., and Mikhailenko, I.A. (1989) Modification of low density lipoprotein by desialylation causes lipid accumulation in cultured cells: discovery of desialylated lipoprotein with altered cellular metabolism in the blood of atherosclerotic patients. *Biochem. Biophys. Res. Commun.*, **162**, 206–211.
- Segrest, J.P., Jones, M.K., Mishra, V.K., Anantharamaiah, G.M., and Garber, D.W. (1994) ApoB-100 has a pentapartite structure composed of three amphipathic alpha-helical domains alternating with two amphipathic beta-strand domains. Detection by the computer program LOCATE. *Arterioscler Thromb.*, **14**, 1674–1685.
- Shireman, R.B. and Fisher, W.R. (1979) The absence of a role for the carbohydrate moiety in the binding of apolipoprotein B to the low density lipoprotein receptor. *Biochim. Biophys. Acta*, **572**, 537–540.
- Taniguchi, T., Ishikawa, Y., Tsunemitsu, M., and Fukuzaki, H. (1989) The structures of the asparagine-linked sugar chains of human apolipoprotein B-100. *Arch. Biochem. Biophys.*, **273**, 197–205.
- Vukmirica, J., Nishimaki-Mogami, T., Tran, K., Shan, J., McLeod, R.S., Yuan, J., and Yao, Z. (2002) The N-linked oligosaccharides at the amino terminus of human apoB are important for the assembly and secretion of VLDL. *J. Lipid. Res.*, **43**, 1496–1507.
- Yang, C.Y., Chen, S.H., Gianturco, S.H., Bradley, W.A., Sparrow, J.T., Tanimura, M., Li, W.H., Sparrow, D.A., DeLoof, H., Rosseneu, M., and others. (1986) Sequence, structure, receptor-binding domains and internal repeats of human apolipoprotein B-100. *Nature*, **323**, 738–742.
- Yang, C.Y., Gu, Z.W., Weng, S.A., Kim, T.W., Chen, S.H., Pownall, H.J., Sharp, P.M., Liu, S.W., Li, H.W., Gotto, A.M. Jr., and Chan, L. (1989) Structure of apolipoprotein B-100 of human low density lipoproteins. *Arteriosclerosis*, **9**, 96–108.